This article has been accepted for publication in a future issue of this journal, but has not been fully edited. Content may change prior to final publication. Citation information: DOI 10.1109/TAP.2020.3028211, IEEE Transactions on Antennas and Propagation

A Dual-Polarized Planar Antenna Array Differentially-Fed by Orthomode Transducer

Qingling Yang, Steven Gao, *Fellow, IEEE*, Qi Luo, *Senior Member, IEEE*, Lehu Wen, Xiaofei Ren, Jian Wu, Yong-Ling Ban, Xuexia Yang, *Senior Member, IEEE*

***Abstract*—This paper presents a new design of a differentially-fed substrate integrated planar antenna array with dual-polarization. Compared with the traditional dual-polarized antenna arrays, the proposed array antenna has the advantages of simple configuration, high cross-polarization discrimination (XPD) and high gain. 2×2-element subarray design with a via-loaded crossover structure is used, which reduces the complexity of the array antenna. The operation bandwidth is improved by generating three resonances in the subarray. An 8×8 antenna array is designed, prototyped and tested to exemplify its potential applications in large dual-polarized antenna arrays. A planar orthomode transducer is used to achieve differential excitation for the antenna array. The measured results show that the proposed antenna array has an impedance bandwidth of 19.2–20.7 GHz for $|S_{11}| < -10$ dB and port isolation higher than 20 dB. The array antenna exhibits a high XPD of 43 dB and a flat gain about 22.2 dBi within the bandwidth.**

***Index Terms*—Antenna array, crossover, cylindrical cavity, differentially-fed, dual-polarized, feed network, orthomode transducer, substrate integrated waveguide (SIW), slot antenna, patch antenna.**

I. Introduction

TO meet the requirements from various scenarios, the wireless communications have increasing demand for high data rate and multi-functionality [1]–[3]. There are a wide variety of solutions to enhance the communication performance [4]–[8]. Among them, dual- or multi-polarization is a good candidate for improving the channel capacity and system reliability. The antenna array with high gain, on the other hand, could achieve higher resolution and increase the transmission range [9], [10]. For some terrestrial and satellite communication systems, the antenna array is also required to have high integration so as to reduce the size, cost and weight of the wireless system.

This work was funded by China Research Institute of Radiowave Propagation, Engineering and Physical Sciences Research Council (EPSRC) under grants EP/P015840/1, EP/N032497/1, and EP/S005625/1. (*Corresponding author: Qingling Yang*)

Q. Yang, S. Gao, and L. Wen are with the School of Engineering and Digital Arts, University of Kent, Canterbury CT2 7NZ, UK.

Q. Luo was with the School of Engineering and Digital Arts, University of Kent, Canterbury CT2 7NZ, U.K. He is now with the Department of Engineering and Technology, University of Hertfordshire, Hatfield AL10 9AB, U.K.

X. Ren and J. Wu are with the China Research Institute of Radiowave Propagation, Xinxiang, Henan 453003, China.

Y. Ban is with the School of Electronic Science and Engineering, University of Electronic Science and Technology of China, Chengdu 611731, China.

X. Yang is with the School of Communication and Information Engineering, Shanghai University, Shanghai 200444, China.

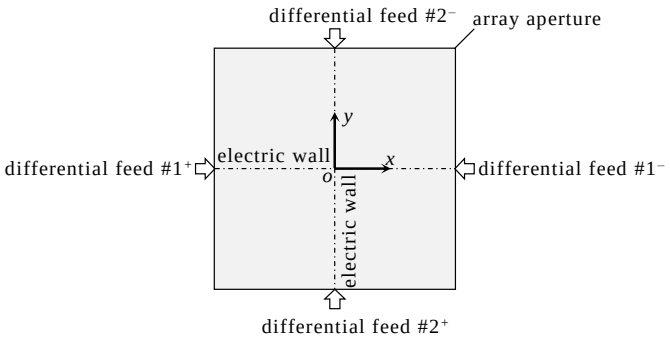

Fig. 1. Diagram of the proposed differentially fed dual-polarized antenna array.

In general, a dual-polarized planar antenna array can be realized with inter-digital or separate orthogonally-polarized linear antenna arrays, as reported in [11]–[13]. However, these antennas have large size and suffer low cross polarization discrimination (XPD). In contrast, the dual-polarized antenna array with shared-aperture is considered as an effective solution to achieve high compactness and high XPD. A considerable number of designs related to this topic have been reported. In [14]–[17], coaxial probe fed patches and Vivaldi antennas are used to design the dual-polarized antenna arrays to achieve wideband operation. The disadvantages of these arrays are high profile and low integration with the RF front-end. In [18], [19], the center and corner patch antenna arrays are designed with the microstrip feed lines on a single laminate, but they have high loss and severe spurious radiation caused by the feed lines. To overcome these problems, the antenna arrays realized by using rectangular waveguides are widely used because they have low insertion loss, high power handling capacity and excellent self-consistent electrical shielding performance. In [20]–[22], the dual-polarized antenna arrays are fed by full corporate waveguides to achieve broadband operation. In [23], series and corporate hybrid feed networks realized with waveguides and striplines are employed to reduce the complexity of the dual-polarized array antenna. However, the downsides of these designs are high profile, low integration and high fabrication cost, etc. In the past twenty years, wide attention has been paid to a planar structure known as the substrate integrated waveguide (SIW) because it inherits the advantages of traditional waveguides and can be fully integrated with other planar circuits by the same processing technology. The typical designs of SIW dual-polarized antenna arrays are found in [24]–[26]. Similar to the waveguide designs reported in [20]–

This article has been accepted for publication in a future issue of this journal, but has not been fully edited. Content may change prior to final publication. Citation information: DOI 10.1109/TAP.2020.3028211, IEEE Transactions on Antennas and Propagation

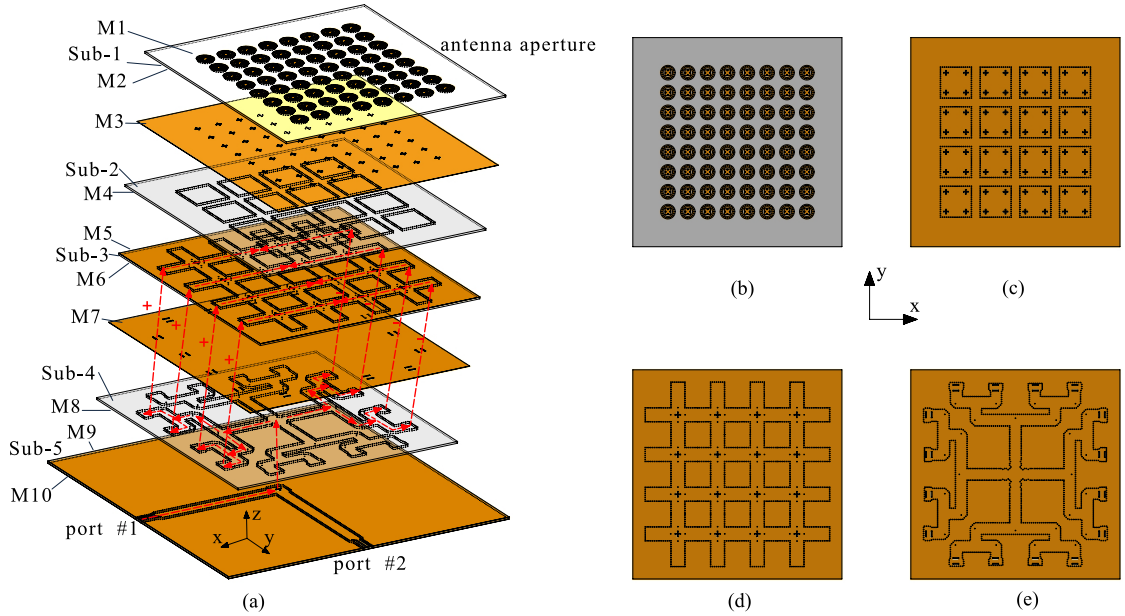

Fig. 2. Configuration of the proposed dual-polarized differentially-fed antenna array. (a) Exploded view. (b) Antenna array aperture. (c) TE_{410} and TE_{140} SIW cavities. (d) Via-loaded crossover structures. (e) Power dividers and orthomode transducer.

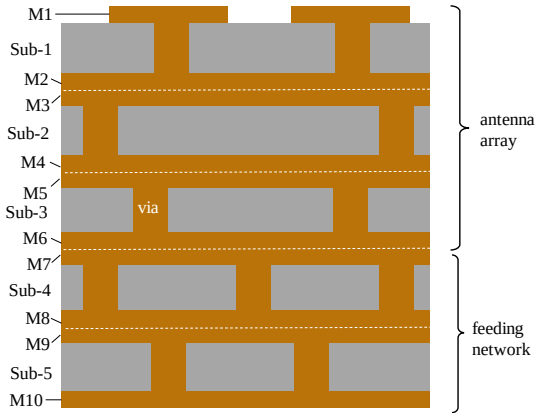

Fig. 3. Cross sectional view of the proposed antenna array.

[23], their feed networks for exciting different polarizations are implemented in separate laminate layers, resulting high complexity and significant loss at high frequencies. In [27], the antenna array realized with SIWs has relatively simple structure compared with the designs in [24]–[26], but it suffers low XPD and poor isolation. A dual-polarized antenna array reported in [28] is designed with its feed networks on a single laminate, but it cannot realize boresight radiation. Designing a dual-polarized array antenna by using parallel plate waveguides is another solution to simplify the design [29], [30]. However, this kind of antenna is only able to operate in a very narrow bandwidth.

As discussed in [23], the series-corporate feed aids in reducing complexity of the dual-polarized antenna array. In this paper, we present a hybrid design solution which incorporates the series feed networks into the design of the dual-polarized antenna elements. To exemplify this concept, an 8×8 antenna array operating at 20 GHz is designed and prototyped. The via-loaded crossover structure is used in the 2×2-element subarray design to enable high isolation between the ports for different polarizations. In order to enhance the operation bandwidth, triple resonance is excited in the subarray antenna. Thanks to the hybrid design approach, the developed antenna array has low complexity, small size and low profile. Moreover, the antenna array exhibits high XPD and high gain. The proposed antenna array is mainly aimed at geostationary satellite communications that can deliver fixed beams for areas with high density of users since dual-polarization and high gain are highly required in such a circumstance.

II. Antenna Array Configuration

Fig. 1 gives the diagram of the proposed differentially fed dual-polarized antenna array. When the differential excitation is imposed at the differential port #1 for horizontal polarization, the *yoz*-plane can be considered as an electric wall because the antenna array is perfectly symmetrical with respect to the *yoz*-plane. In this case, differential port #2 is well isolated to the differential-mode signal input from differential port #1. Besides, differential port #2 is also isolated to common-mode signal because differential port #2 is located along the electric wall in the *yoz*-plane. Thus, the isolation between differential ports #1 and #2 can be improved. In this proposed antenna array, because of high structure symmetry and differential feed, the radiated cross-polarized waves are equal in magnitude but opposite in phase with respect to the electric walls. This leads to destruction of cross-polarization radiations in the far field; thus high XPD can be obtained in the proposed antenna array. In this design, differential feeds to the antenna array are produced by an orthomode transducer. Fig. 2 shows the configuration of the proposed

This article has been accepted for publication in a future issue of this journal, but has not been fully edited. Content may change prior to final publication. Citation information: DOI 10.1109/TAP.2020.3028211, IEEE Transactions on Antennas and Propagation

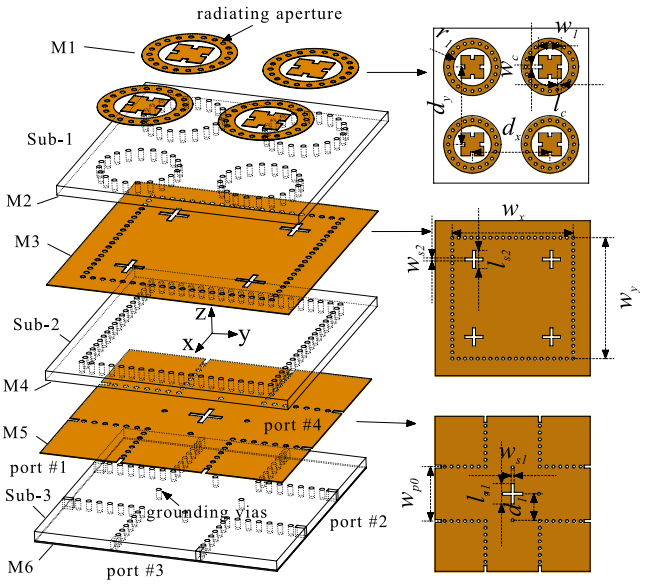

Fig. 4. Configuration of the 2×2 element subarray. (Dimensions: $w_{p0} = 7.2$ mm, $l_{s1} = 2.9$ mm, $w_{s1} = 0.4$ mm, $d_1 = 3.5$ mm; $l_{s2} = 2.4$ mm, $w_{s2} = 0.4$ mm, $w_x = 16$ mm, $w_y = 16$ mm; $r_1 = 3.2$ mm, $w_1 = 3$ mm, $l_c = 0.5$ mm, $w_c = 0.4$ mm, $d_x = 10.25$ mm, $d_y = 10.25$ mm)

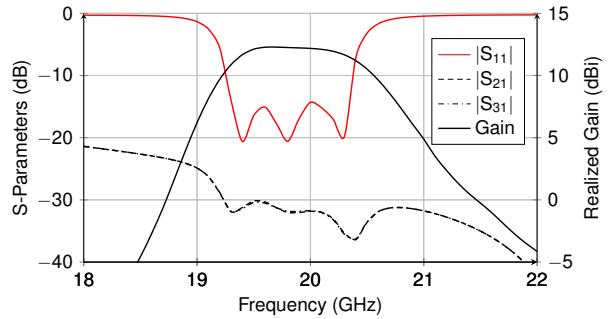

Fig. 5. Simulated S-parameters and gain of the designed 2×2-element subarray.

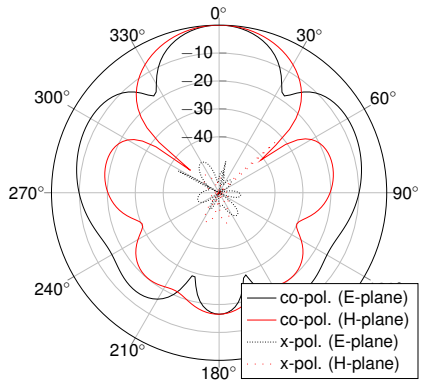

Fig. 6. Normalized radiation patterns of the designed 2×2-element subarray.

dual-polarized differentially-fed array antenna, and its cross sectional view is shown in Fig. 3. Five double-sided laminates are used in the design, and they are screwed together with screws for convenience of assembling. Sub-1 to Sub-5 are the dielectric layers, and M1 to M10 are the copper layers. In this antenna array, there are 8×8 radiating elements and they are designed on the copper layer M1. These radiating elements are able to work with dual-polarization, and they are uniformly separated in the x- and y-axis direction. Every 2×2 antenna element is defined as a subarray and shares one SIW cavity supporting TE_{410} and TE_{140} modes on laminate Sub-2. Within these cavities, four cross slots are etched on the top copper layer of laminate Sub-2 to excite the 2×2 antenna elements. The TE_{410} and TE_{140} mode cavity is driven by a cross slot designed on the copper layers M4 and M5. On the laminate Sub-3, four horizontal SIWs are perpendicular to another four parallel SIWs. Around each junction of any two SIWs, four grounding vias are placed to enable the signals from orthogonal directions travel across the junction without interference. The red dashed arrows in Fig. 2(a) represent the signal paths in the feed network when port #1 is excited. Signals are coupled from Sub-5 to Sub-4 by a cross slot etched on the copper layers M8 and M9. They are equally split by the orthomode transducer, and then they flow to the power dividers along the x-axis direction with out-of-phase. The differential signals are then coupled from the slots etched on the copper layers M6 and M7 to excite the antenna array. The antenna array is designed on the upper three laminate layers, and the feed networks are realized on the lower two laminates. All the laminates used in this design are the Rogers RO4003 with a thickness of 0.813 mm, relative permittivity of 3.55 and the loss tangent of 0.0027. The simulations in this work are performed with the high frequency full-wave electromagnetic solver, ANSYS Electronic Desktop HFSS 19.

III. Antenna Design

A. 2×2-Element Subarray

Fig. 4 shows the configuration of the 2×2-element subarray. Four resonant patches are placed inside the cylindrical cavities with a radius of r_1. They are separated in the x- and y-axis direction with a distance of $d_x = d_y = 0.68\lambda_0$. The antenna elements are excited by the cross slots etched over the SIW cavity supporting TE_{140} and TE_{410} modes in the laminate Sub-2. This cavity is excited by a cross slot etched over a crossover structure designed on the laminate Sub-3. The crossover structure is a four-port component, which enables the subarray to be excited from the x- and y-axis direction for dual-polarization. Four metallized vias, which help realize high isolation between any two orthogonal ports, are placed around the junction of the crossover. In this simulation, to obtain the impedance characteristics of the subarray antenna, port #2 is disabled by a short circuit when port #1 is excited [31]. The periodic boundary condition is imposed to the sub-array considering the mutual couplings between the subarrays.

The simulated performances of the subarray are illustrated in Fig. 5 and Fig. 6. The impedance bandwidth for $|S_{11}| < -10$ dB is from 19.3 GHz to 20.5 GHz. The subarray exhibits good port isolation between port #1 and #3, which is higher than 30 dB within this bandwidth. Stable gain with a variation from 10.8 dBi to 12.2 dBi is observed over the impedance bandwidth. Outside this bandwidth, the gain decreases to less than 0 dBi at 18.8 GHz and 21. 2 GHz. The simulated radiation patterns of the subarray are shown in Fig. 6, where symmetric patterns are observed in both the E-plane (yoz-plane) and H-plane (xoz-plane). The XPD is higher

This article has been accepted for publication in a future issue of this journal, but has not been fully edited. Content may change prior to final publication. Citation information: DOI 10.1109/TAP.2020.3028211, IEEE Transactions on Antennas and Propagation

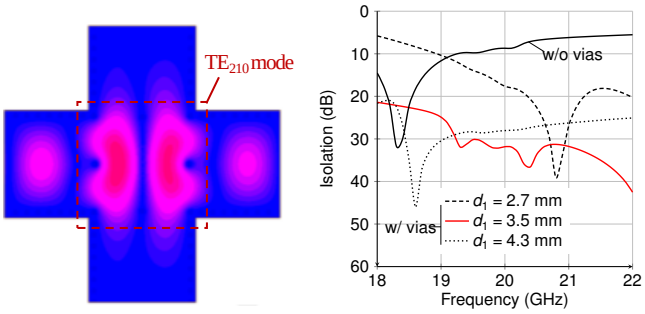

(a) (b)

Fig. 7. (a) Field distribution inside the crossover. (b) Simulated isolation of the crossover designed with and without the four grounding vias around the junction.

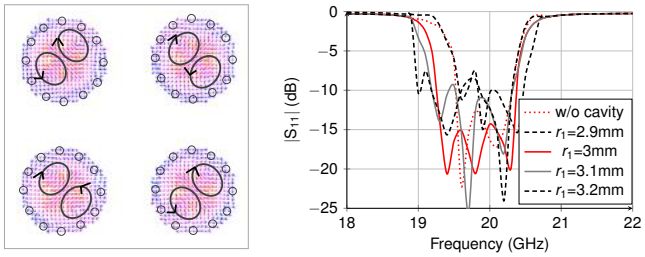

(a) (b)

Fig. 8. (a) Magnetic field distribution inside the cylindrical cavities at 20 GHz. (b) Simulated $|S_{11}|$ with different cavity size r_1.

than 58 dB, and the front-to-back ratios of the co-polarization patterns are 17 dB in the two planes.

B. Via-Loaded Crossover

The crossover structure, located in the laminate Sub-3, plays an important role in designing the dual-polarized antenna array. It enables the signals to travel in the linear subarrays without interference from other parallel linear subarrays. It is composed of two perpendicular SIWs with a width of w_{p0}. An SIW cavity is formed by placing four grounding vias around the junction. To realize good isolation between the ports for different polarizations, only the degenerate TE_{210} and TE_{120} modes are allowed in the cavity [28]. The fundamental mode and other higher order modes are suppressed within the operation bandwidth by adjusting the via position d_1. The size of this cavity is $2d_1 \times 2d_1 = 7$ mm $\times$ 7 mm, which is smaller than a fully enclosed SIW cavity supporting TE_{210} and TE_{120} modes with the same frequency.

Fig. 7(a) shows the electric field distribution inside the crossover with port #1 excited. Due to the presence of the four grounding vias, the TE_{210} mode field is observed in the junction of the crossover. It can be seen that the electromagnetic waves are well constrained when they travel through the junction. High isolation is achieved between port #1 and #3 or #4. Fig. 7(b) gives the simulated isolation between ports #1 and #3 of the crossover designed with and without the four grounding vias. Over the operation bandwidth (19.3–20.5 GHz), the isolation between ports #1 and #3 is lower than 10 dB if the crossover is designed with no grounding vias loaded around its junction. It is worth noting that the

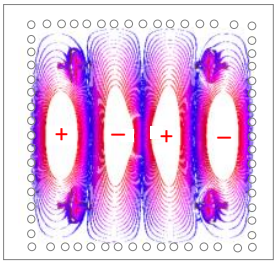

Fig. 9. Simulated electric field inside the square SIW cavity.

port isolation of the crossover is substantially improved after inserting four vias around the junction. The isolation increases to higher than 30 dB over the operation bandwidth when the via position d_1 is 3.5 mm. The via position is a key parameter in determining the isolation, because it significantly affects the mode field inside the junction of the crossover. As can be seen from Fig. 7(b), with d_1 increasing from 2.7 mm to 4.3 mm, the port isolation increases firstly then decreases after reaching the maximum 31 dB when $d_1 = 3.5$ mm.

C. Triple Resonance

In this developed subarray, three resonance modes are obtained over the operation bandwidth. The first resonance at 19.5 GHz is caused by the SIW cylindrical cavity. As demonstrated in [32], a cylindrical cavity can act as an aperture radiator when it operates with TM_{110} mode. For a cylindrical cavity with a radius of r_1 and a height of h, the resonant wavelength of TE_{mnp} and TM_{mnp} modes is formulated by [33]

$$\left(\frac{2r_1}{\lambda}\right)^2 = K_c + \frac{p^2}{4}\left(\frac{2r_1}{h}\right)^2 \tag{1}$$

where K_c is the mode constant and has two different series of values for TE and TM modes. It can be calculated by

$$K_c = \left(\frac{u_{mn}}{\pi}\right)^2 \tag{2}$$

where u_{mn} is the n^{th} root of $J'_m(x) = 0$ for TE modes, and u_{mn} is the n^{th} root of $J_m(x) = 0$ for TM modes. $J_m(x)$ is the Bessel function of the first kind of order n. The order of modes varies with r_1 and h. In this design, only TM_{110} mode is excited in the cylindrical cavity, because the diameter of the cavity is limited to less than one wavelength for the purpose of compactness. In addition, in practical applications, the thickness of the laminate used in antenna design should be no more than half a wavelength in order to prevent surface waves. As a result, the modes in the z-direction of the cylindrical cavity is suppressed. By solving (1) and (2), the initial resonance frequency of the cylindrical cavity can be obtained.

Fig. 8(a) shows the magnetic field distribution inside the cylindrical cavities of the subarray at 20 GHz. It is seen that the TM_{110} mode field patterns rotate $+45°$ or $-45°$ with respect to the center of each cavity. Broadside radiation can be obtained from the subarray as the magnetic field among the cavities is anti-symmetric. Fig. 8(b) compares the $|S_{11}|$ of the subarray antenna designed with and without the cylindrical cavity. As can be seen from this figure, the

This article has been accepted for publication in a future issue of this journal, but has not been fully edited. Content may change prior to final publication. Citation information: DOI 10.1109/TAP.2020.3028211, IEEE Transactions on Antennas and Propagation

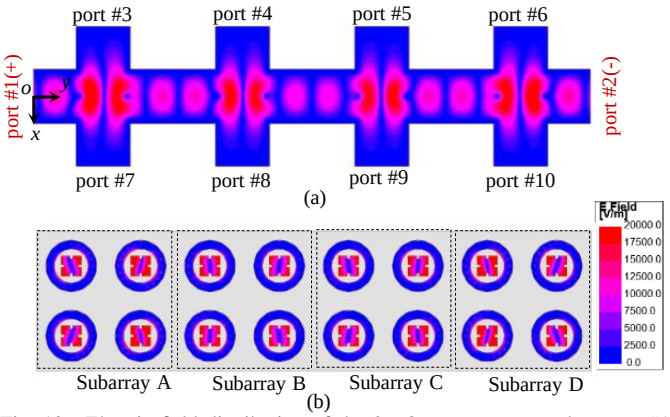

Fig. 10. Electric field distribution of the 2×8 antenna array when port #1 and #2 are excited differentially at 20 GHz. (a) Field distribution in the SIW crossover. (b) Field distribution at the radiating aperture.

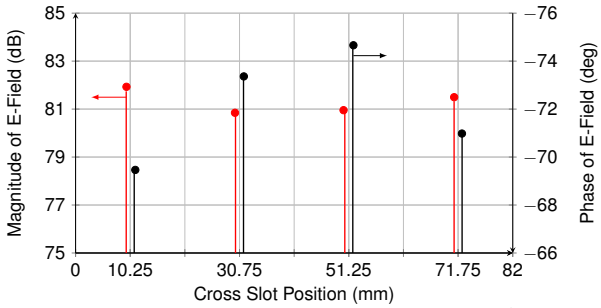

Fig. 11. Simulated magnitude and phase of the electric fields $\vec{E}_y$ at the centre of the cross slots.

antenna designed without the cylindrical cavity shows good performance in a relatively narrow band. Two resonances are observed at 19.6 GHz and 20.1 GHz, which are caused by the patch and the cross slot below the patch, respectively. After the cylindrical cavity is employed in the subarray, an additional resonance is introduced. The resonance moves to the lower band as r_1 increases, resulting in an improved operation bandwidth of the antenna. The presence of the cylindrical cavity also affects the resonance frequencies caused by the patch and the cross slot since the cavity is very close to these structures. The two resonances shift to the lower frequency band when the cylindrical cavity is enlarged. When $r_1 = 3$ mm, the impedance bandwidth for $|S_{11}|$ less than –10 dB is achieved in the frequency range 19.3–20.5 GHz.

As discussed, the second resonance at 19.8 GHz and the third resonance at 20.3 GHz are generated by the patch inside the cylindrical cavity and the cross slot below the patch, respectively. As to the resonant patch, four rectangular slits with the dimension of $w_c \times l_c$ are cut along the centre line in order to extend the current path while without increasing the patch size. The cross slot with a length of l_{s2} below the patch is etched over an square SIW cavity supporting TE_{410} and TE_{140} modes in the laminate Sub-2. The position of the cross slots relative to the centre of the TE_{410} mode cavity in x- and y-axis direction is $d_x/2 = d_y/2 = 0.34\lambda_0$. The resonance frequency of a rectangular or square cavity supporting the designated

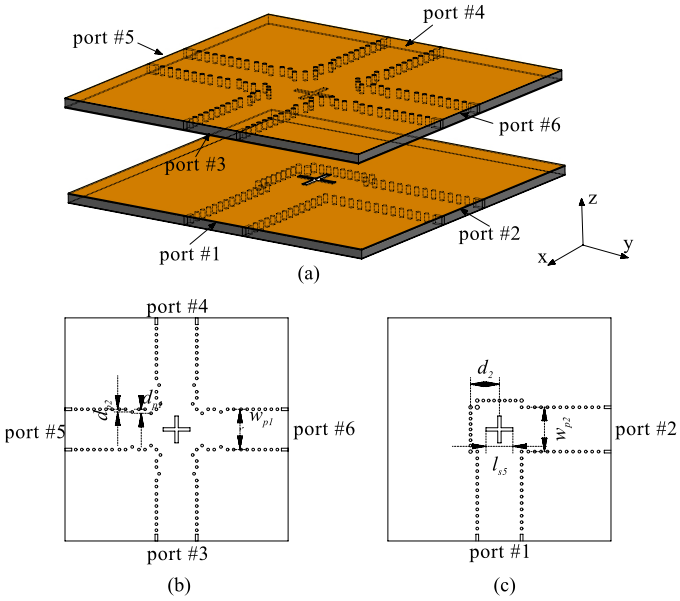

Fig. 12. Designed planar orthomode transducer. (a) Exploded view. (b) Top laminate. (c) Bottom laminate. (Dimensions: $w_{p1} = 6$ mm, $d_{p1} = 0.94$ mm, $d_{p2} = 0.53$ mm; $w_{p2} = 6.6$ mm, $d_1 = 4.76$ mm, $l_{s5} = 4.8$ mm.)

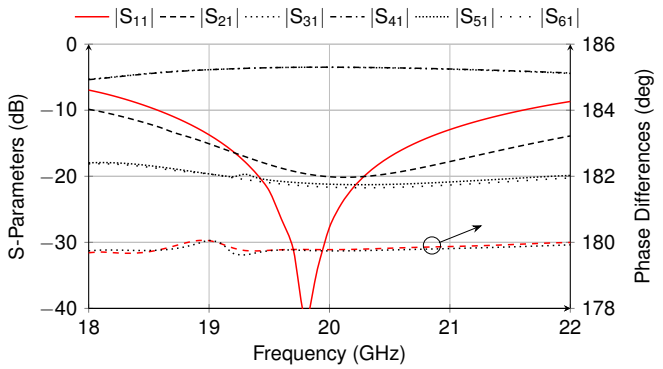

Fig. 13. Simulated performance of the designed planar orthomode transducer.

TE_{mn0} mode is given by [34]

$$f_{mnp} = \frac{c}{2\pi\sqrt{\varepsilon_r}}\sqrt{\left(\frac{m\pi}{w_x}\right)^2 + \left(\frac{n\pi}{w_y}\right)^2} \tag{3}$$

where w_x and w_y are the length and width of the cavity, respectively. In this design, the SIW cavity is a square one ($w_x = w_y$) in order to make sure that the TE_{410} and TE_{140} mode fields inside the cavity have the same resonance frequency. By substituting the resonance frequency in (3), the initial cavity size can be obtained. Fig. 9 gives the simulated TE_{410} mode field distribution inside the square SIW cavity. The signs $'+'$ and $'-'$ denote the direction of electric field along the z-axis. The cross slots are enabled to resonate in-phase as they are located at the same position relative to the centre of the cavity. Finally, good impedance matching over an improved operation bandwidth 19.3–20.5 GHz is realized by optimizing the parameters r_1, l_c and l_{s2}.

D. 2×8 *Antenna Array*

In order to exemplify the performance of the subarray, a 2×8 antenna array with a series combination of four

This article has been accepted for publication in a future issue of this journal, but has not been fully edited. Content may change prior to final publication. Citation information: DOI 10.1109/TAP.2020.3028211, IEEE Transactions on Antennas and Propagation

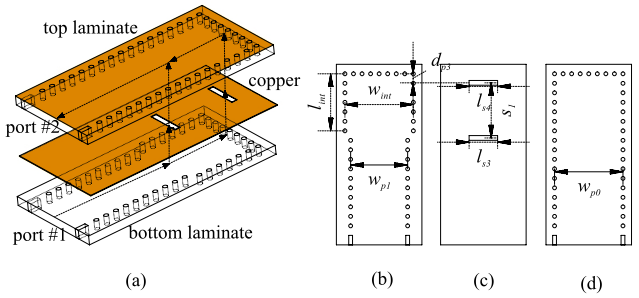

Fig. 14. 180° SIW elbow. (a) Exploded view. (b) Bottom laminate. (c) Coupling slots in the copper layer. (d) Top laminate. (Dimensions: $w_{p1} = 6$ mm, $w_{int} = 7.2$ mm, $l_{int} = 3.2$ mm, $d_{p3} = 0.8$ mm, $l_{s3} = l_{s4} = 3$ mm, $s_1 = 2.95$ mm, $w_{p0} = 7.2$ mm.)

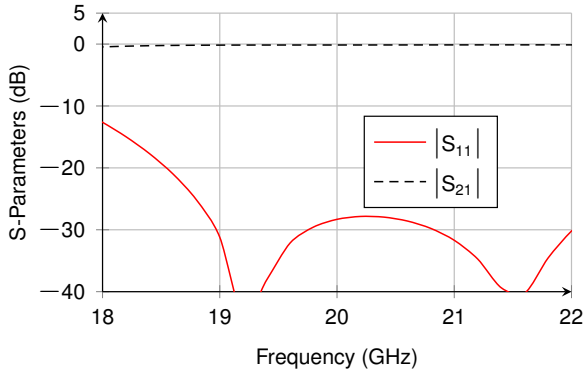

Fig. 15. Simulated *S*-parameters of the designed 180° SIW elbow.

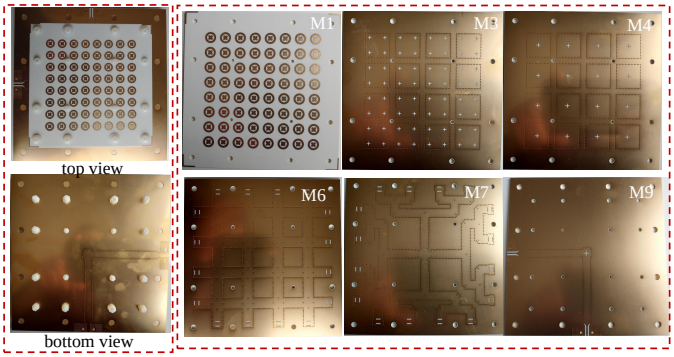

Fig. 16. Prototype of the antenna array. (a) Top and bottom view of the antenna array. (b) Different copper layers of the antenna array.

2×2-element subarrays is investigated. In this antenna array, differential feed is imposed at ports #1 and #2, and ports #3 – #10 are terminated with a matched load. In this antenna array, the separations between the antenna elements are larger than $0.5\lambda_0$. This is because a) the physical size of the square cavity should be more than $1\lambda_0$ so as to support TE_{410} and TE_{140} modes, b) the length of the SIW connected to the crossover needs to be tuned and thus the element separation should be further increased in order to realize in-phase uniform excitation among the elements. Fig. 10(a) shows the simulated electric field distribution in the crossover structures of the antenna array. It is observed that the fields are constrained along the horizontal direction and ports #3–#10 are well isolated when differential excitation is imposed at ports #1 and #2. The TE_{120} mode field is clearly seen in each junction of the crossovers. These phenomena indicate that the signals can travel in the linear crossover structures without interference to other parallel antenna arrays. To have a better understanding of the field uniformity, a field probe is added at the centre of each cross slot in the simulation. Fig. 11 gives the simulated magnitude and phase of the electric fields $\vec{E}_y$ at the centre of the cross slots. The four cross slots are located at y = 10.25 mm, y = 30.75 mm, y = 51.25 mm and y = 71.75 mm, respectively. Differential feed is imposed at y = 0 mm and y = 82 mm. As can be seen from Fig. 11, the magnitude of extracted electric fields at these locations is 81.74 dB, 80.85 dB, 80.94 dB and 81.33 dB, and the phase of extracted electric fields is $-69.54°$, $-73.45°$, $-74.64°$ and $-70.87°$, respectively. Thus, from the extracted electric fields it can be concluded that these subarrays are excited with almost the equal magnitude and the same phase. The cross slot etched over the crossover couples EM waves to excite the cavity supporting TE_{140} and TE_{410} modes and then drive the radiating elements. Uniform and in-phase field distribution is observed among the radiating elements, as shown in Fig. 10(b).

IV. Feed Networks

A. Planar Orthomode Transducer

Fig.12 shows the configuration of the designed planar orthomode transducer. It is realized by using two laminate layers where the top laminate includes a four-port junction and the bottom laminate includes two feed ports. Interlayer transmission is achieved by etching a cross slot on the copper layer between the two laminates. The orthomode transducer can be considered as a six-port differential network or a polarization duplexer [27], [35], [36]. It is often used to combine or to separate two orthogonally polarized waves received by or transmitted from a differentially-fed dual-polarized antenna. Ports #1 and #2 are the feed ports. Ports #3 and #4, and ports #5 and #6 are two differential feed pairs used to excite the antenna array for dual-polarization. When port #1 is excited, signals are coupled from the bottom laminate to the top laminate by the cross slot, and are split by the junctions, and then exit at port #3 and #4 with out-of-phase. Ideally, ports #2, #5 and #6 are isolated from port #1, and ports #1, #3 and #4 are isolated from port #2.

The simulated results of the designed orthomode transducer are shown in Fig. 13. The impedance bandwidth of $|S_{11}|$ less than –15 dB is 19.1–20.7 GHz. Good isolation between port #1 and port #5 or #6 is achieved by optimizing the size of the cross junction and the offsets of the metalized vias, d_{p1} and d_{p2}. Within the frequency range 19–22 GHz, $|S_{51}|$ and $|S_{61}|$ are less than –20 dB. The $|S_{21}|$ is less than –15 dB in the bandwidth from 19 GHz to 21.6 GHz, and at 20 GHz this value is less than –22 dB. The isolation between ports #1 and #2 is mainly affected by the semi-open SIW cavity in the bottom laminate. The phase differences between ports #3 and #4, ports #5 and #6 are also included in Fig. 13. Over the bandwidth from 18 GHz to 22 GHz, the phase differences are with a variation from 179.6° to 180.1°, indicating that the differential excitation for the antenna array is achieved.

This article has been accepted for publication in a future issue of this journal, but has not been fully edited. Content may change prior to final publication. Citation information: DOI 10.1109/TAP.2020.3028211, IEEE Transactions on Antennas and Propagation

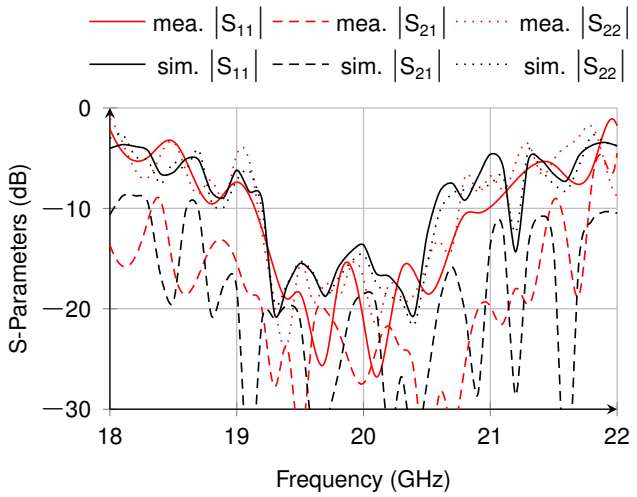

Fig. 17. Measured and simulated *S*-parameters of the designed dual-polarized antenna array.

B. 180° SIW Elbow for Interlayer Transmission

As can be seen from Fig. 2, the connections between the antenna array and each four-way power dividers are realized by using four 180° SIW elbows. The configuration of the 180° SIW elbow is presented in Fig. 14, where port #1 is connected to the power divider and port #2 is connected to the antenna array. Interlayer transmission is realized by etching two transverse slots on the copper layers between the two laminates. In order to improve the impedance bandwidth, the separation between the two transverse slots is designed to be around $\lambda/4$. From the simulation, the designed 180° SIW elbow has lower insertion loss and wider operation bandwidth than the 180° SIW elbow with only one transverse slot. In addition, the width of the SIW near the end-wall in the bottom laminate is increased from w_{p1} to w_{int} so as to reduce the return loss. The simulated performance of the designed 180° SIW elbow is shown in Fig. 15. The insertion loss from port #1 to #2 is lower than 0.22 dB and the impedance bandwidth for $|S_{11}|$ less than –30 dB is achieved in the frequency range 19–21 GHz.

V. Measurement and Results

The proposed antenna array was prototyped and measured to verify the design concept. Fig. 16(a) gives the top and bottom view of the fabricated antenna, and Fig. 16(b) shows the different copper layers constructing the design. Only copper layers M1, M3, M4, M6, M7 and M9 are presented in Fig. 16(b), since back-to-back coppers layers have the same etched patterns. All the laminate layers of the antenna prototype were stacked up and then screwed together with screws. To reduce board-to-board misalignment as much as possible, proper alignment marks and densely enough screw holes are added to each laminate layers. The measurement of *S*-parameters of the antenna array is conducted by using the network analyzer Anritsu 37397C, and the radiation patterns are measured in the far-field anechoic chamber.

A. Impedance Bandwidth and Port Isolation

Fig. 17 shows the measured and simulated $|S_{11}|$, $|S_{22}|$ and $|S_{21}|$ of the proposed antenna array. It is seen that the measured results are in good agreement with the simulations. The overlapped impedance bandwidth for $|S_{11}|$ and $|S_{22}|$ less than –10 dB ranges from 19.2 GHz to 20.7 GHz. The measured isolation between port #1 and #2 is higher than 20 dB over this bandwidth.

B. Radiation Patterns and Gain

Fig.18(a)-(c) shows the measured and simulated radiation patterns of the designed antenna array at 19.2 GHz, 20 GHz and 20.6 GHz when port #1 is excited for vertical polarization. It can be seen that the calculated and the measured patterns are in good agreement at both the *xoz*- and *yoz*-plane. Due to the limitation of the measurement system, radiation patterns out of the range $-90^\circ < \varphi < 90^\circ$ are not measured. It is observed that the antenna array exhibits good radiation performance with the main beam at the boresight. The radiation patterns are very similar in the two planes and keep stable over the operation bandwidth. The XPD measures 43 dB at the boresight. The first sidelobe levels (SLLs) are –14 dB in the *xoz*- and *yoz*-plane. Similar radiation patterns are obtained when port # 2 is excited for horizontal polarization, as shown in Fig. 18(d)-(f).

Fig. 19 shows the simulated and measured realized gains of the antenna array. The antenna array exhibits a flat gain about 22.2 dBi from 19.2 GHz to 20.6 GHz when port #1 is excited. The measured realized gains are in good agreement with the simulated ones. The antenna array reaches to its maximum measured realized gain 22.8 dBi at 19.9 GHz. At 19 GHz and 21.1 GHz, the realized gain is suppressed to less than 5 dBi. Similar tendency of the realized gain varied with frequency is observed when port #2 is excited. The simulated radiation efficiency of the antenna is higher than 61% over the operation bandwidth and reaches to the peak 72% at 19.9 GHz.

C. Comparison and Discussion

Table. I compares the proposed antenna array with other reported dual-polarized array antennas. In this table, the aperture efficiency of an antenna is given by [31]

$$\eta_{ap} = \frac{G_{max}\lambda_0^2}{4\pi A_{ap}} \tag{4}$$

where G_{max} and A_{ap} are the maximum realized gain and the physical dimension of the antenna, respectively. The antenna array in [12] is realized with the feed networks on a single laminate. However, it has large size and very low aperture efficiency. The antenna in [16] has wide bandwidth, but it has low XPD and high profile. To avoid congestion of feed networks, the feed networks for exciting different polarization in [23]–[25] are designed on separate laminate layers. Thus, these antennas have very high complexity. The antennas in [27] and [29] has relatively simple configuration. But the antenna in [27] suffers low XPD, and the antenna in [29] has very narrow bandwidth and low aperture efficiency. The proposed antenna has low complexity since the series feed networks are

This article has been accepted for publication in a future issue of this journal, but has not been fully edited. Content may change prior to final publication. Citation information: DOI 10.1109/TAP.2020.3028211, IEEE Transactions on Antennas and Propagation

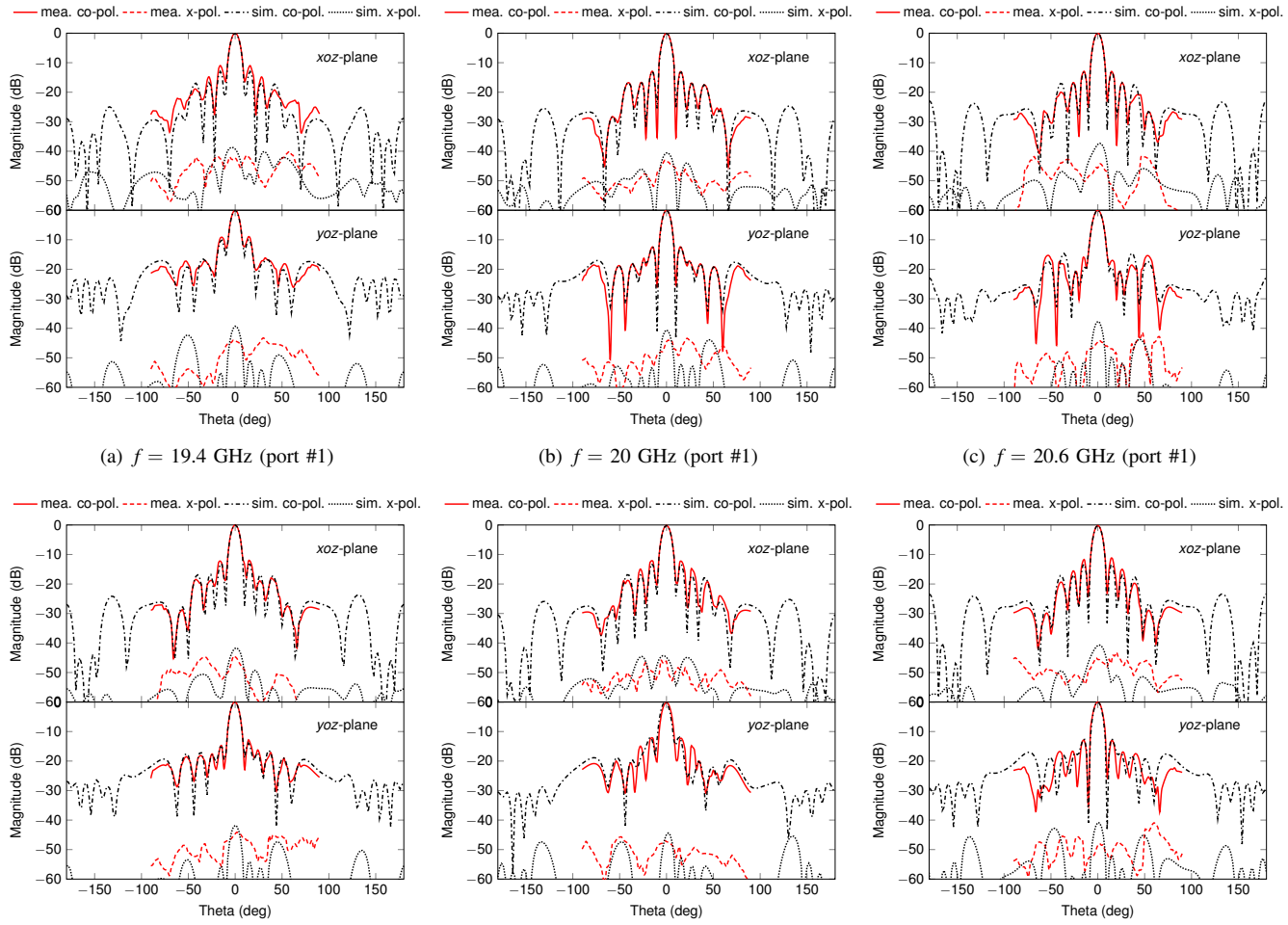

(a) $f = 19.4$ GHz (port #1) (b) $f = 20$ GHz (port #1) (c) $f = 20.6$ GHz (port #1)

(d) $f = 19.4$ GHz (port #2) (e) $f = 20$ GHz (port #2) (f) $f = 20.6$ GHz (port #2)

Fig. 18. Normalized far-field radiation patterns at the frequencies 19.4 GHz, 20 GHz and 20.6 GHz when port #1 or port #2 is excited.

TABLE I
COMPARISON BETWEEN THE PROPOSED ANTENNA AND THE REPORTED DUAL-POLARIZED ANTENNA ARRAYS

Ref.	BW	Antenna Element	XPD	No. of Elements	G_{max}	Feed Network	Fabrication	thickness (λ_0)	η_{ap}
[12]	1.5%	slot	25 dB	11×12	22.2 dBi	series-corporate, low complexity	PCB	0.14	22%
[16]	22.2%	Vivaldi	18 dB	8×8	n.a.	probe feed, low complexity	CNC	1.1	n.a.
[23]	13.2%	aperture	27 dB	8×8	26 dBi	series-corporate, high complexity	CNC	2.7	75%
[24]	17.1%	cavity-backed slot	20 dB	8×8	22.3 dBi	full-corporate, high complexity	PCB	0.47	46%
[25]	12.2%	aperture	30 dB	8×8	19.6 dBi	full-corporate, high complexity	LTCC	0.29	50%
[27]	23%	patch	15 dB	8×8	25.8 dBi	full-corporate, low complexity	PCB	0.7	69%
[29]	1.1%	long slot	n.a.	15×15	26 dBi	series-corporate, low complexity	PCB	0.32	30%
This work	7.5%	cavity-backed slot coupled patch	43 dB	8×8	22.8 dBi	series-corporate, low complexity	PCB	0.27	51%

incorporated into the design of antenna elements. In addition, by using the simplified feed networks and the differential feed technique, the proposed antenna has significant improvement in performance compared with other reported works. As summarized in Table. I, the developed antenna shows the advantages of high XPD, high aperture efficiency, low profile, and ease of fabrication.

This article has been accepted for publication in a future issue of this journal, but has not been fully edited. Content may change prior to final publication. Citation information: DOI 10.1109/TAP.2020.3028211, IEEE Transactions on Antennas and Propagation

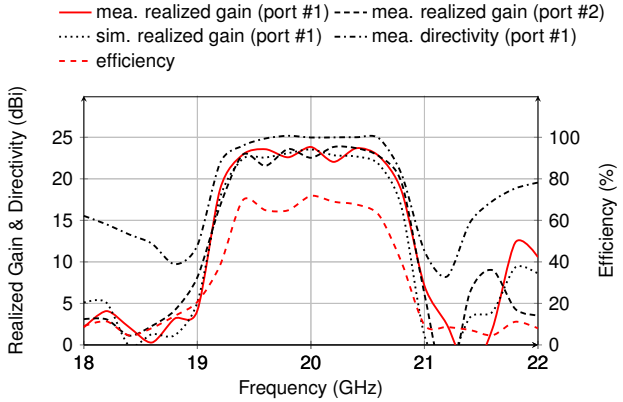

Fig. 19. Realized gain, directivity, efficiency of the antenna array.

VI. Conclusion

This paper presents a novel design of shared-aperture dual-polarized antenna array differentially fed by an orthomode transducer. Compared with the traditional designs, the structure of the proposed antenna array is greatly simplified as the series feed networks are incorporated into the design of the subarrays. A via-loaded crossover is introduced into the design. To enhance the operation bandwidth, triple resonance is excited in the subarray. The design principles and procedures are described in detail. An 8×8 antenna array operating in 19.2–20.7 GHz is prototyped and tested to exemplify the concept. The results show that the array antenna has the advantages of stable patterns, high XPD (43 dB) and high gain (22.8 dBi). In addition, it can be easily manufactured by using PCB technology with low cost. The developed dual-polarized antenna array is a good candidate for geostationary satellite communications that produces fixed beams for areas with high density of users and devices.

References

[1] R. Deng, S. Xu, F. Yang, and M. Li, "An FSS-backed Ku/Ka quad-band reflectarray antenna for satellite communications," *IEEE Trans. Antennas Propag.*, vol. 66, no. 8, pp. 4353–4358, 2018.

[2] D. Raychaudhuri and N. B. Mandayam, "Frontiers of wireless and mobile communications," *Proc. IEEE*, vol. 100, no. 4, pp. 824–840, 2012.

[3] M. Xiao, S. Mumtaz, Y. Huang, L. Dai, Y. Li, M. Matthaiou, G. K. Karagiannidis, E. Bjrnson, K. Yang, C. I, and A. Ghosh, "Millimeter wave communications for future mobile networks," *IEEE J. Sel. Areas Commun.*, vol. 35, no. 9, pp. 1909–1935, 2017.

[4] S. Chen, J. Row, and K. Wong, "Reconfigurable square-ring patch antenna with pattern diversity," *IEEE Trans. Antennas Propag.*, vol. 55, no. 2, pp. 472–475, 2007.

[5] C. B. Dietrich, K. Dietze, J. R. Nealy, and W. L. Stutzman, "Spatial, polarization, and pattern diversity for wireless handheld terminals," *IEEE Trans. Antennas Propag.*, vol. 49, no. 9, pp. 1271–1281, 2001.

[6] Y. Dong and T. Itoh, "Planar ultra-wideband antennas in Ku- and K-band for pattern or polarization diversity applications," *IEEE Trans. Antennas Propag.*, vol. 60, no. 6, pp. 2886–2895, 2012.

[7] C. Mao, Z. H. Jiang, D. H. Werner, S. S. Gao, and W. Hong, "Compact self-diplexing dual-band dual-sense circularly polarized array antenna with closely spaced operating frequencies," *IEEE Trans. Antennas Propag.*, vol. 67, no. 7, pp. 4617–4625, 2019.

[8] Y. Wu, C. Wu, D. Lai, and F. Chen, "A reconfigurable quadri-polarization diversity aperture-coupled patch antenna," *IEEE Trans. Antennas Propag.*, vol. 55, no. 3, pp. 1009–1012, 2007.

[9] P. R. Grajek, B. Schoenlinner, and G. M. Rebeiz, "A 24-GHz high-gain Yagi-Uda antenna array," *IEEE Trans. Antennas Propag.*, vol. 52, no. 5, pp. 1257–1261, 2004.

[10] A. I. Sandhu, E. Arnieri, G. Amendola, L. Boccia, E. Meniconi, and V. Ziegler, "Radiating elements for shared aperture Tx/Rx phased arrays at K/Ka band," *IEEE Trans. Antennas Propag.*, vol. 64, no. 6, pp. 2270–2282, 2016.

[11] J. Lu, H. Zhang, W. Wang, X. Liang, J. Ge, M. Jin, and W. Wu, "Broadband dual-polarized waveguide slot filtenna array with low cross polarization and high efficiency," *IEEE Trans. Antennas Propag.*, vol. 67, no. 1, pp. 151–159, 2019.

[12] Sehyun Park, Y. Okajima, J. Hirokawa, and M. Ando, "A slotted post-wall waveguide array with interdigital structure for 45° linear and dual polarization," *IEEE Trans. Antennas Propag.*, vol. 53, no. 9, pp. 2865–2871, 2005.

[13] Y. Yu, W. Hong, Z. H. Jiang, and H. Zhang, "E -band low-profile, wide-band 45° linearly polarized slot-loaded patch and its array for millimeter-wave communications," *IEEE Trans. Antennas Propag.*, vol. 66, no. 8, pp. 4364–4369, 2018.

[14] A. Garcia-Aguilar, J. Inclan-Alonso, L. Vigil-Herrero, J. Fernandez-Gonzalez, and M. Sierra-Perez, "Low-profile dual circularly polarized antenna array for satellite communications in the X band," *IEEE Trans. Antennas Propag.*, vol. 60, no. 5, pp. 2276–2284, 2012.

[15] C. Wang, Y. Chen, and S. Yang, "Dual-band dual-polarized antenna array with flat-top and sharp cutoff radiation patterns for 2G/3G/LTE cellular bands," *IEEE Trans. Antennas Propag.*, vol. 66, no. 11, pp. 5907–5917, 2018.

[16] H. Khknen, J. Ala-Laurinaho, and V. Viikari, "Dual-polarized Ka-band Vivaldi antenna array," *IEEE Trans. Antennas Propag.*, vol. 68, no. 4, pp. 2675–2683, 2020.

[17] J. Yan, S. Gogineni, B. Camps-Raga, and J. Brozena, "A dual-polarized 2–18-GHz Vivaldi array for airborne radar measurements of snow," *IEEE Trans. Antennas Propag.*, vol. 64, no. 2, pp. 781–785, 2016.

[18] Y. Zhang and J. Li, "A differential-series-fed dual-polarized traveling-wave array for full-duplex applications," *IEEE Trans. Antennas Propag.*, pp. 1–1, 2019.

[19] Shun-Shi Zhong, Xue-Xia Yang, Shi-Chang Gao, and Jun-Hai Cui, "Corner-fed microstrip antenna element and arrays for dual-polarization operation," *IEEE Trans. Antennas Propag.*, vol. 50, no. 10, pp. 1473–1480, 2002.

[20] S. Zhou, G. Huang, T. Chio, J. Yang, and G. Wei, "Design of a wideband dual-polarization full-corporate waveguide feed antenna array," *IEEE Trans. Antennas Propag.*, vol. 63, no. 11, pp. 4775–4782, 2015.

[21] J. Wu, Y. J. Cheng, H. B. Wang, Y. C. Zhong, D. Ma, and Y. Fan, "A wideband dual circularly polarized full-corporate waveguide array antenna fed by triple-resonant cavities," *IEEE Trans. Antennas Propag.*, vol. 65, no. 4, pp. 2135–2139, 2017.

[22] D. Kim, M. Zhang, J. Hirokawa, and M. Ando, "Design and fabrication of a dual-polarization waveguide slot array antenna with high isolation and high antenna efficiency for the 60 GHz band," *IEEE Trans. Antennas Propag.*, vol. 62, no. 6, pp. 3019–3027, 2014.

[23] G. Huang, S. Zhou, T. Chio, C. Sim, and T. Yeo, "Waveguide-stripline series-corporate hybrid feed technique for dual-polarized antenna array applications," *IEEE Trans. Compon. Packag. Manuf. Technol.*, vol. 7, no. 1, pp. 81–87, 2017.

[24] Z. Chen, H. Liu, J. Yu, and X. Chen, "High gain, broadband and dual-polarized substrate integrated waveguide cavity-backed slot antenna array for 60 GHz band," *IEEE Access*, vol. 6, pp. 31 012–31 022, 2018.

[25] P. Li, S. Liao, Q. Xue, and S. Qu, "60 GHz dual-polarized high-gain planar aperture antenna array based on LTCC," *IEEE Trans. Antennas Propag.*, vol. 68, no. 4, pp. 2883–2894, 2020.

[26] C. Wu, H. Wang, X. Jiang, S. Quan, and X. Liu, "High-gain dual-polarization higher order mode substrate integrated cavity antenna array," *2016 11th International Symposium on Antennas, Propagation and EM Theory (ISAPE)*, pp. 129–131, 2016.

[27] Y. Zhao and K. Luk, "Dual circular-polarized SIW-fed high-gain scalable antenna array for 60 GHz applications," *IEEE Trans. Antennas Propag.*, vol. 66, no. 3, pp. 1288–1298, 2018.

[28] Q. Yang, S. Gao, Q. Luo, L. Wen, Y. Ban, X. Yang, X. Ren, and J. Wu, "Dual-polarized crossed slot array antenna designed on a single laminate for millimeter-wave applications," *IEEE Trans. Antennas Propag.*, vol. 68, no. 5, pp. 4120–4125, 2020.

[29] Y. J. Cheng, J. Wang, and X. L. Liu, "94 GHz substrate integrated waveguide dual-circular-polarization shared-aperture parallel-plate long-slot array antenna with low sidelobe level," *IEEE Trans. Antennas Propag.*, vol. 65, no. 11, pp. 5855–5861, 2017.

[30] X. Lu, H. Zhang, S. Gu, H. Liu, X. Wang, and W. Lu, "A dual-polarized cross-slot antenna array on a parallel-plate waveguide with compact structure and high efficiency," *IEEE Antennas Wireless Propag. Lett*, vol. 17, no. 1, pp. 8–11, 2018.

[31] R. S. Elliot, *Antenna Theory and Design*. Hoboken: John Wiley & Sons, 1981.

[32] M. Li, K. A. Hummer, and K. Chang, "Theoretical and experimental study of the input impedance of the cylindrical cavity-backed rectangular slot antennas," *IEEE Trans. Antennas Propag.*, vol. 39, no. 8, pp. 1158–1166, 1991.

[33] R. N. Bracewell, "Charts for resonant frequencies of cavities," *Proc. IEEE*, vol. 35, no. 8, pp. 830–841, 1947.

[34] H. B. Wang and Y. J. Cheng, "Broadband printed-circuit-board characterization using multimode substrate-integrated- waveguide resonator," *IEEE Trans. Antennas Propag.*, vol. 65, no. 6, pp. 2145–2152, 2017.

[35] A. Navarrini and R. L. Plambeck, "A turnstile junction waveguide orthomode transducer," *IEEE Trans. Microw. Theory Techn.*, vol. 54, no. 1, pp. 272–277, 2006.

[36] M. Esquius-Morote, M. Mattes, and J. R. Mosig, "Orthomode transducer and dual-polarized horn antenna in substrate integrated technology," *IEEE Trans. Antennas Propag.*, vol. 62, no. 10, pp. 4935–4944, 2014.